Cancer Research

Downregulation of Human DAB2IP Gene Expression in Prostate Cancer Cells Results in Resistance to Ionizing Radiation

Zhaolu Kong[1,5], Daxing Xie[2], Thomas Boike[1], Pavithra Raghavan[1], Sandeep Burma[1,4], David J. Chen[1,4], Amyn A. Habib[3,4], Arup Chakraborty[6], Jer-Tsong Hsieh[2,4,7], and Debabrata Saha[1,4]

Abstract

DAB2IP (DOC-2/DAB2 interactive protein) is a member of the RAS-GTPase–activating protein family. It is often downregulated in metastatic prostate cancer and has been reported as a possible prognostic marker to predict the risk of aggressive prostate cancer. In this study, we furnish several lines of evidence indicating that metastatic human prostate cancer PC3 cells deficient in DAB2IP (shDAB2IP) exhibit increased clonogenic survival in response to ionizing radiation (IR) compared with control cells expressing an endogenous level of DAB2IP (shVector). Radioresistance was also observed in normal prostate cells that are deficient in DAB2IP. This enhanced resistance to IR in DAB2IP-deficient prostate cancer cells is primarily due to faster DNA double-strand break (DSB) repair kinetics. More than 90% of DSBs were repaired in shDAB2IP cells by 8 hours after 2 Gy radiation, whereas only 60% of DSB repair were completed in shVector cells at the same time. Second, upon irradiation, DAB2IP-deficient cells enforced a robust G_2-M cell cycle checkpoint compared with control cells. Finally, shDAB2IP cells showed resistance to IR-induced apoptosis that could result from a striking decrease in the expression levels of proapoptotic proteins caspase-3, caspase-8, and caspase-9, and significantly higher levels of antiapoptotic proteins Bcl-2 and STAT3 than those in shVector cells. In summary, DAB2IP plays a significant role in prostate cell survival following IR exposure due to enhanced DSB repair, robust G_2-M checkpoint control, and resistance to IR-induced apoptosis. Therefore, it is important to identify patients with dysregulated DAB2IP for (*a*) assessing prostate cancer risk and (*b*) alternative treatment regimens. *Cancer Res; 70(7); 2829–39. ©2010 AACR.*

Introduction

Prostate cancer represents the most common incidence of cancers and the second leading cause of cancer-related death in U.S. men. Specifically, prostate cancer accounts for 25% of diagnosed cancers in U.S. men and 10% of cancer-related death (1). Current medical management for localized prostate cancer ranges from close monitoring for indolent disease to radical treatment such as radiation or surgery. Treatment with radiation therapy has the advantage of being noninvasive and well tolerated. However, a significant proportion of high-risk patients will fail therapy and develop metastatic disease, for which no curative treatment currently exists (2, 3). Increasing our understanding about biomarkers and their effect on therapeutic response may allow physicians to personalize care based on the patient's biomarkers in the future.

A recent study by Duggan and colleagues (4) offers a new single nucleotide polymorphism marker from the *DAB2IP* gene that can predict aggressive prostate cancer. DAB2IP is a novel member of the Ras GTPase–activating protein family and is often downregulated in prostate cancer (5). By knocking down endogenous DAB2IP levels, prostate cancer cells could gain proliferative potential and become resistant to stress-induced apoptosis (6). Most importantly, the loss of DAB2IP expression in prostate epithelia leads to epithelial-mesenchymal transition, a central step in tumor metastasis, through recruitment of PP2A and GSK-3β resulting in β-catenin degradation. All these findings support a tumor suppressive role of DAB2IP (7) in prostate cancer development.

Therefore, it is important to understand the response to ionizing radiation (IR) of DAB2IP-deficient prostate cancer cells. Our results clearly show that the loss of DAB2IP expression in prostate cancer and normal prostate epithelia results in resistance to IR. This, in sum, is due to more efficient

Authors' Affiliations: Departments of [1]Radiation Oncology, [2]Urology, and [3]Neurology, University of Texas Southwestern Medical Center; and [4]Simmons Comprehensive Cancer Center, Dallas, Texas; [5]The Institute of Radiation Medicine, Fudan University, Shanghai, China; [6]College of Pharmacy, University of Southern Nevada, Henderson, Nevada; and [7]Graduate Institute of Cancer Biology, China Medical University, Taichung, Taiwan, Republic of China

Note: Supplementary data for this article are available at Cancer Research Online (http://cancerres.aacrjournals.org/).

D. Xie and T. Boike contributed equally to this work.

Corresponding Author: Debabrata Saha, Department of Radiation Oncology, Division of Molecular Radiation Biology, University of Texas Southwestern Medical Center, 2201 Inwood Road, Dallas, TX 75390-9187. Phone: 214-648-7750; Fax: 214-648-5995; E-mail: debabrata.saha@utsouthwestern.edu.

doi: 10.1158/0008-5472.CAN-09-2919

©2010 American Association for Cancer Research.

Downloaded from http://aacrjournals.org/cancerres/article-pdf/70/7/2829/2645522/2829.pdf by guest on 16 January 2025

repair, robust cell cycle checkpoint activation, and decreased apoptosis. To the best of our knowledge, this is the first report to suggest a link between the expression of DAB2IP and radiation sensitivity.

Materials and Methods

Cell culture. PC3 and its derivative lines were maintained in T medium supplemented with 5% FCS, 100 U/mL penicillin, 100 μg/mL streptomycin, 900 μg/mL of G418, and 700 ng/mL of Puromycin in a humidified atmosphere with 5% carbon dioxide. RWPE-1 cell, a normal prostatic epithelial cell line derived from the peripheral zone of prostate gland and immortalized by human papillomavirus (HPV) 18 virus, was maintained in Keratinocyte KSF medium (Invitrogen Corp.) with 10% fetal bovine serum. PZ-HPV-7 cell is a normal prostatic epithelial cell line derived from a donor with cystoprostectomy by immortalizing with HPV18. All the knockdown and control sublines from these cell lines were generated using the shRNA-lentiviral system (Open Biosystems) under puromycin selection. DAB2IP-transfected C4-2 subline-D_2 and its vector control subline-Neo were also maintained in T medium with 5% FCS, 1% pencicilin+streptomycin, and 400 μg/mL of G418.

Irradiation. All cells were irradiated at room temperature in ambient air using a 137Cs source (Mark 1-68 irradiator, JL Shepherd & Associated) at a dose rate of 3.47 Gy/min.

Antibodies. Anti–phospho-Histone γH2AX (Ser139) and anti–phospho-Histone H3 (Ser 10) were from Millipore; signal transducers and activators of transcription 3 (STAT3) and 53BP1 antibodies were from Cell Signaling Technology, Inc.; anti–caspase-3, caspase-8, and caspase-9 were from EMD Chemicals, Inc.; and anti–Bcl-2 and the horseradish peroxidase–conjugated secondary antibodies against mouse and rabbit were obtained from Santa Cruz Biotechnology, Inc. Actin antibody was purchased from Sigma-Aldrich, Inc. Fluorescent dye–conjugated secondary antibodies were obtained from Invitrogen Corp.

Clonogenic survival. Exponentially growing cells were trypsinized and counted using a particle counter (Beckman Coulter, Inc.). Cells were diluted serially to appropriate concentrations and plated into 60-mm dish in triplicate for 2 h. Then, cells were treated with increasing doses of IR (0, 2, 4, 6, and 8 Gy). After 7 or 14 d of incubation, the colonies were fixed and stained with 4% formaldehyde in PBS containing 0.05% crystal violet. Colonies containing >50 cells were counted. Surviving fraction was calculated as (mean colony counts)/[(cells inoculated) × (plating efficiency)], in which plating efficiency was defined as (mean colony counts)/(cells inoculated for unirradiated controls). The data are presented as the mean ± SEM of at least three independent experiments. The curve $S = e - (\alpha D + \beta D2)$ was fitted to the experimental data using a least square fit algorithm using the program Sigma Plot 11.0 (Systat Software, Inc.).

Limiting dilution assay. Both C4-2 Neo and D2 cells were serially diluted with different concentrations of 10,000, 5,000, 2,500, 1,250, 625, 300, 150, and 125 cells per 100 μL. Using a multichannel pipette, 100 μL of each dilution were transferred onto 8 wells of a 96-well dish. Separate plates were prepared for 0, 2, 4, and 6 Gy and the experiments were repeated thrice. Cells were allowed adhere to the plastic. Within 4 to 6 h following plating, cells were exposed to the appropriate dose of radiation using ^{137}Cs irradiator. Following irradiation, plates were transferred to the incubator and allowed to form colonies for 10 d. At the end of the growth period, cells were fixed with 4% formaldehyde, 10% methanol, and Giemsa; thoroughly washed; and wells were examined for colonies using an inverted microscope. A colony is defined as a compact cluster of cells with at least 50 cells. Positive wells (those that contained at least one colony) and negative wells [those that did not contain any colony, had one or more abortive colonies (with fewer than 50 cells), or had multiple cells stuck to the plate with no visible signs of clonogenic growth] were counted. After correcting for residual error between plates and experiments, and based on the assumption of 100% clonogenic efficiency, relative survival was calculated as the ratio of cell number resulting in 50% positive wells in irradiated samples to the cell number providing 50% positive wells in unirradiated samples according to Green and colleagues (8). Curves obtained by plotting relative surviving fraction as a function of radiation dose were then fitted to the linear quadratic equation using Sigma Plot 11.0 (Systat Software, Inc.).

Double-strand break repair assay. A double-strand break (DSB) repair assay was done by counting the colocalized 53BP1 and phospho-γH2AX foci after radiation (9, 10). Cells were plated on poly-lysine–coated coverslips, were allowed to attach, and were exposed to total dose of 2 Gy radiation. Cells were fixed in 4% formaldehyde/PBS for 30 min, permeabilized in 0.5% Triton X-100 in PBS for 1 h, and blocked in 5% bovine serum albumin and 1% normal goat serum for 1 h at room temperature. Then, cells were incubated with the primary antibody, anti–phospho-Histone γH2AX (Ser139; 1:2,000), and anti-53BP1 (1:1,500) for 1 h. Alexa Fluor 488–conjugated goat anti-Rabbit and rhodamine red–conjugated goat anti-mouse were used as secondary antibodies. Cells were mounted in a Vectashield mounting medium containing 4′,6-diamidino-2-phenylindole (DAPI). Phospho-γH2AX and 53BP1 foci were examined using a fluorescence microscope (CRG Precision Electronics). The number of merged 53BP1 and phospho-γH2AX foci (yellow) was determined at each time point (average of 50 nuclei), and after subtracting background (number of foci in unirradiated population), the percentage foci remaining was plotted against time to obtain DSB repair kinetics.

Comet assay. The frequency of DSBs and single-strand breaks in PC3 shDAB2IP and shVector cells post-IR were compared by using the alkaline comet assay kit (Trevigen, Inc.). Briefly, cells were plated on 60-mm dishes, were allowed to attach, and were exposed to total radiation dose of 2 Gy. After treatment, cells were collected at different times as indicated mixed with low-melting-point agarose and were spread onto Comet slides. The slides were left to dry for 15 min at 4°C then dipped in prechilled lysis solution for 30 min followed by alkaline buffer treatment for 30 min at 4°C. The slides were subjected to electrophoresis (300 mmol/L NaOH, 1 mmol/L

Downloaded from http://aacrjournals.org/cancerres/article-pdf/70/7/2829/2645522/2829.pdf by guest on 16 January 2025

EDTA) for 20 min at a voltage of 0.5 V/cm. Next, the slides were rinsed with neutralization buffer [20 mmol/L Tris (pH 7.4)] for 20 min. Finally, each slide was stained with 100 μg/mL propidium iodide (PI). PI-stained nuclei were observed and photographed using a fluorescence microscope (CRG Precision Electronics) and images of a minimum of 50 cells per treatment were analyzed using the Casp software. In the present study, tail moment [%DNA in tail × by tail length (μm)] were used as parameters to assess DNA damage.

Cell cycle and early G_2-M checkpoint assay. Dual parameter flow cytometry method was used as follows: PI staining for DNA content and anti–Phospho-Histone H3 for detecting the % of mitosis cells. Cells were plated in 100-mm dishes overnight and samples were collected as described. Briefly, the medium was collected to recover floating cells and attached cells were harvested by trypsinization and mixed with the pool of floating cells at 2, 4, and 8 h after exposure to 2 and 5 Gy IR. After fixing and incubation with anti–phospho-Histone H3 (Ser 10), cells were stained with Alexa Fluor 488–conjugated anti-rabbit secondary antibody and PI, and analyzed on a flow cytometer (BD FACScans). Three independent experiments were done and at least 20,000 cells were counted, the proportion of cells of different phase was gated and calculated using the software Flowjo 8.7.1(Tree Star, Inc.).

Apoptosis assay. Cells were plated in a 100-mm dish and treated with indicated dosage of radiation on the second day. Floating and attached cells were harvested at 24 and 48 h postradiation. After centrifugation (200 × *g*, 5 min), the medium was removed and the cell pellet was carefully resuspended in 5 mL PBS. Phycoerythrin Annexin V apoptosis detection kit I (BD Biosciences) was used to identify apoptotic cells by flow cytometry. Cells that stain positive for Phycoerythrin Annexin V and negative for 7-AAD (right bottom quadrant) are undergoing apoptosis. Cells treated with 5 mmol/L sodium butyrate (NaBu) for 24 h were applied as positive control of apoptosis (11, 12). The proportion of apoptosis cells were gated and calculated by Flowjo 8.7.1.

Western blot assay. Cell lysates were prepared from each sample with a lyses buffer [50 mmol/L Tris (pH 7.5), 1% NP40, 1 mmol/L EDTA] and a cocktail of protease and phosphotase inhibitors (1 mmol/L phenylmethylsulfonylfluoride, 0.2 mmol/L sodium orthovanadate, 0.1 mmol/L sodium fluoride, 10 μg/mL aprotinin, and 10 μg/mL leupeptin). Protein concentration was quantified by Bradford assay (Bio-Rad). An equal amount of total protein (20 μg) was subjected to a 10% SDS-PAGE and transferred to polyvinylidene difluoride membranes and probed with primary antibodies as indicated. Actin was used for loading control.

Statistical analysis. The data are presented as the mean ± SEM of at least three independent experiments. The results were tested for significance using the unpaired Student's *t* test.

Results

Decreased DAB2IP expression enhances radioresistance. To determine the role of DAB2IP in prostate cancer cells after IR, endogenous DAB2IP of a metastatic prostate cancer cell line (PC3) was knocked down using shRNA-lentiviral system and Western blot analysis was done to show the loss of DAB2IP protein expression in DAB2IP knockdown (shDAB2IP) cells compared with the control (shVector) cells (Fig. 1A). Both derivative lines were exposed to increasing doses of IR (0, 2, 4, 6, and 8 Gy). Radiation caused a dose-dependent reduction in the clonogenic survival in both lines. However, shDAB2IP cells showed higher radioresistance compared with shVector cells (Fig. 1B). The surviving fraction at 2 Gy (SF_2) of shDAB2IP and shVector cells were 0.64 ± 0.04 and 0.38 ± 0.05, respectively (Supplementary Table. S1A; Fig. 1B). We also measured the cell proliferation rate based on MTT assay following increasing doses of IR (0–10 Gy) in both sublines (Fig. 1C and D). shDAB2IP cells clearly showed a greater proliferation rate than shVector cells even at higher radiation dose (Fig. 1D). Because DAB2IP is a member of the GTPase-activating protein family inhibiting the Ras-mediated signal pathway, we used a ras signaling pathway inhibitor (FTI-277) to study the radiosensitization in the DABIP-deficient and control cells (Supplementary Fig. S1). Our results showed that FTI-277 caused significant radiosensitization in DAB2IP-deficient cells (SF2, 0.53 ± 0.01) compared with the DAB2IP-proficient cells (SF2, 0.36 ± 0.01).

To further characterize the role of DAB2IP in radioresistance, two human immortalized normal prostate epithelial cell lines PZ-HPV-7 and RWPE-1 were subjected to clonogenic survival assay (Fig. 2). Again, the endogenous DAB2IP expression was knocked down using shRNA-lentiviral system (Fig. 2A). shDAB2IP sublines from both PZ-HPV-7 and RWPE-1 cells showed more radioresistance compared with shVector cells. SF_2 values of the shDAB2IP sublines from PZ-HPV-7 and RWPE-1 were 0.73 ± 0.01 and 0.64 ± 0.03, respectively, compared with 0.51 ± 0.03 and 0.42 ± 0.01 in the shVector cells, respectively, (Supplementary Table S1B and C; Fig. 2B and C). In another experiment, we further characterized the role of DAB2IP in radiosensitization by overexpressing DAB2IP in C4-2 prostate cancer cells (D_2-Cells; Fig. 2A). Because the plating efficiency of D2 and vector control (Neo-cells) sublines of C4-2 are extremely low, we did a limiting dilution assay (Fig. 2D) following the method described by Green and colleagues (8). We noticed that after the overexpression of DAB2IP protein, C4-2 cells became more radiosensitive; SF_2 values of the D_2 and Neo were 0.43 ± 0.01 versus 0.76 ± 0.07 (Supplementary Table S1D; Fig. 2D). Taken together, these results indicate that the down-regulation of DAB2IP significantly enhances IR resistance in both prostate cancer and normal prostate epithelial cells.

DAB2IP knockdown–induced IR resistance is associated with enhanced DSB repair in PC3 cells. Enhanced DSB repair is an important mechanism by which cells may become resistant to IR (13, 14). To measure the induction and repair of IR-induced DSBs, shDAB2IP and shVector cells were exposed to a total dose of 2 Gy and samples were collected at the indicated times (Fig. 3A). An early step in DSB repair involves the rapid phosphorylation of γH2AX and recruitment of 53BP1 that form foci at the damage sites (9, 10, 15–17). Cells were subjected to dual immunofluorescence staining for 53BP1 (green) and phospho-γH2AX (red) foci, and DSB repair kinetics were determined by counting the colocalized foci (yellow).

Downloaded from http://aacrjournals.org/cancerres/article-pdf/70/7/2829/2645522/2829.pdf by guest on 16 January 2025

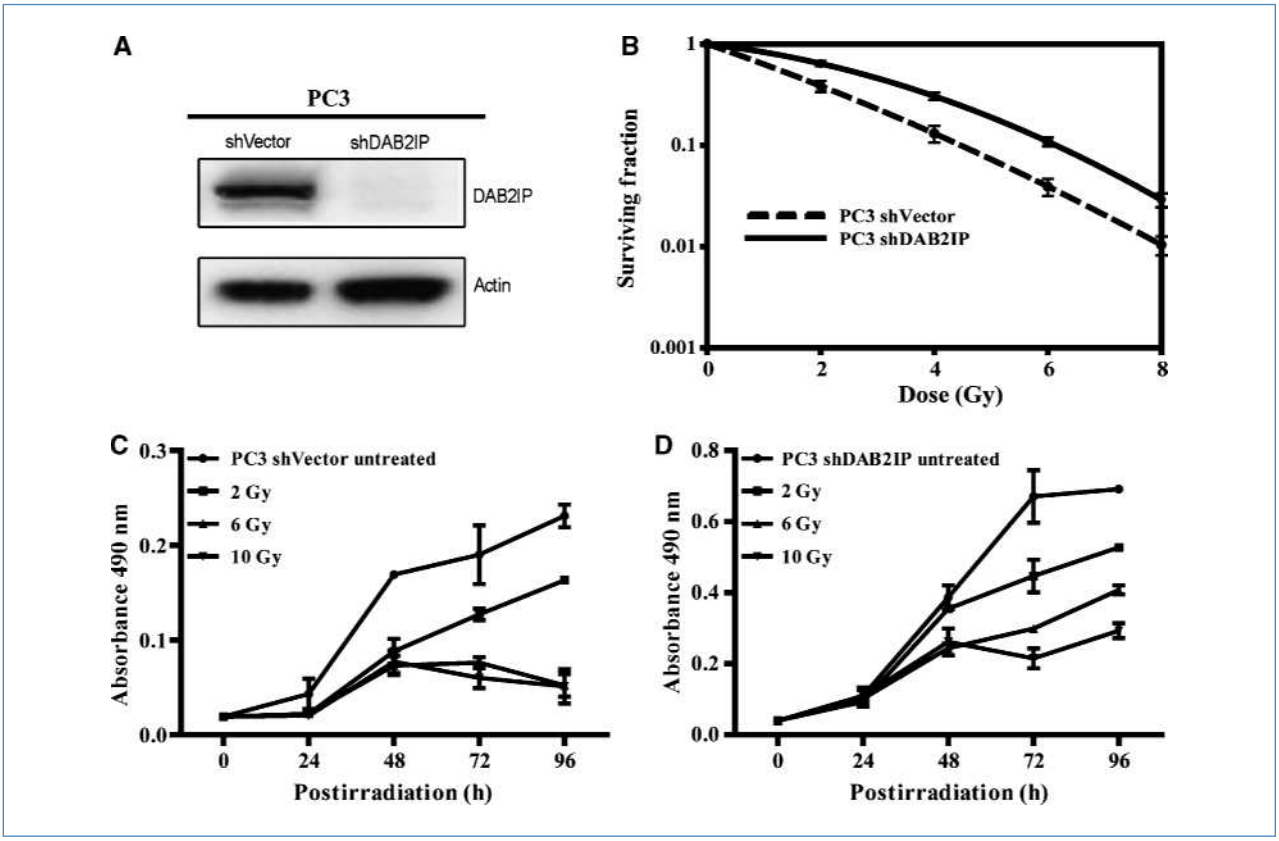

Figure 1. Decreased DAB2IP expression increases radioresistance in prostate cancer cells. A, detection of DAB2IP protein in PC3 shVector and PC3 shDAB2IP cells. A rabbit polyclonal DAB2IP antibody (1:250) was used for Western blot analysis. B, clonogenic survival of shDAB2IP and shVector cells. Cells were exposed to increasing doses of radiation as indicated. After 7 to 14 d, colonies were counted and survival curves were constructed by fitting mean values from three independent experiments to a linear-quadratic model. Results were obtained from three independent experiments and compared in Supplementary Table S1A with Student's *t* test ($P < 0.01$). C to D, viability assay of shDAB2IP and shVector cells in response to radiation. C, shVector; D, shDAB2IP. Cells were plated in triplicates in 96-well plates and MTT assay was done to determine the cell viability 24, 48, 72, and 96 h postradiation. Absorbance at wavelength of 490 nm were measured by using Microplate Reader (BioTek Instruments).

We observed a significantly faster rate of DSB repair in shDAB2IP cells compared with shVector cells (Fig. 3B). More than 90% repair was completed at 8 hours following IR in shDAB2IP cells, whereas shVector cells still retained nearly 60% and 40% of foci at 8 and 24 hours, respectively. These data indicate that knockdown of DAB2IP in PC3 cells is associated with accelerated DSB repair kinetics (Fig. 3B). Based on surviving fraction analysis and DSB repair kinetics, it is now clear that DAB2IP level modulates radiosensitization. In an additional experiment, we applied alkaline single cell gel electrophoresis (Fig. 3C and D) to quantify the DNA damage in the DAB2IP-deficient and DAB2IP-proficient cells in response to a radiation dose of 2 Gy. We observed an extended migration of the fragmented DNA in the comet tails of both DAB2IP-proficient and DAB2IP-deficient cells at 30 minutes post-IR. Tail moment (%DNA in tail × tail length) was then used to evaluate the level of DNA damage (18). In DAB2IP-deficient cells, the mean value of tail moment decreased to basal levels within 8 hours post-IR, suggesting that the loss of DAB2IP significantly enhances the repair of radiation-induced damage (Fig. 3D, inset). In contrast, the mean tail moment was significantly high even after 24 hours postirradiation in the DAB2IP proficient cells (Fig. 3C, inset).

DAB2IP knockdown cells exhibit a robust early G_2-M checkpoint after IR. In mammalian cells, IR induces blocks in the G_1, S, and G_2 phases and these cell cycle checkpoints are necessary to maintain genomic stability. In this study, we determined the G_2 block in both derivative lines by flow cytometric analysis of histone H3 phosphorylation. This assay specifically distinguishes the cells entering M phase from G_2 cells with a G_2-M block manifesting as a decrease in the M phase population (19). Results in Fig. 4 indicate that >90% of shDAB2IP cells are blocked in G_2 within 2 hours of a total radiation dose of 2 Gy (4.04 ± 0.11% to 0.40 ± 0.01%). These cells again reenter mitosis within 4 hours (0.40 ± 0.01% to 4.19 ± 0.14%) after radiation. In contrast, shVector cells continue to enter mitosis even 2 hours after radiation with only 50% decrease in the M phase population, indicating a G_2-M block that is less robust that seen upon DAB2IP knockdown. Taken together, these results indicate that the robust G_2-M checkpoint and accelerated DSB repair might render shDAB2IP cells more radioresistant than shVector cells.

Downloaded from http://aacrjournals.org/cancerres/article-pdf/70/7/2829/2645522/2829.pdf by guest on 16 January 2025

DAB2IP knockdown cells are resistant to radiation-induced apoptosis. Clearly, the shDAB2IP cells showed an increased resistance to IR due to the enforcement of the early G_2-M check and efficient DNA repair. In addition, we examined the IR-induced apoptotic response in shDAB2IP cells. Using Annexin V/7-AAD staining, we noticed that at 2 Gy, shDAB2IP cells did not undergo apoptosis until 48 hours post-IR (Fig. 5*A*). On the other hand, >18% Annexin V–positive cells were detected in the shVector population compared with <1% cells in the shDAB2IP population when cells were not treated with radiation (Fig. 5*A*). But no further apoptosis was noticed in both cell lines in response to IR. As a positive control, NaBu was used to detect apoptotic cells (11, 12). We observed extensive apoptosis (40%) after a 24-hour treatment of NaBu only in shVector cells not in the shDAB2IP cells. Interestingly, NaBu caused significant necrosis in shDAB2IP cells at the same time point (Fig. 5A). We then tested the effect of higher radiation dose (10 Gy) specifically on shDAB2IP cells at 24, 48, and 72 hours post-IR (Supplementary Fig. S3). Our results showed no significant induction of IR-induced apoptosis even after 72 hours, whereas, on the other hand, necrotic cell populations was greatly increased in shDAB2IP cells at 48 and 72 hours post-IR (Supplementary Fig. S3). To further characterize apoptosis in these sublines, Western blot analysis was done (Fig. 5B). Interestingly, we noticed that the basal expression levels of critical proapoptotic proteins such as caspase-3, caspase-9, and caspase-8 were significantly higher in shVector cells than shDAB2IP cells, whereas the antiapoptotic proteins STAT3 and Bcl-2 levels were elevated in shDAB2IP cells (Fig. 5B). Furthermore, there were no detectable changes in expression of these proteins upon radiation in shDAB2IP cells (data not shown). These data provide evidence indicating that shDAB2IP cells may have an additional survival advantage due to elevated expression of antiapoptotic proteins and reduced expression of proapoptotic proteins.

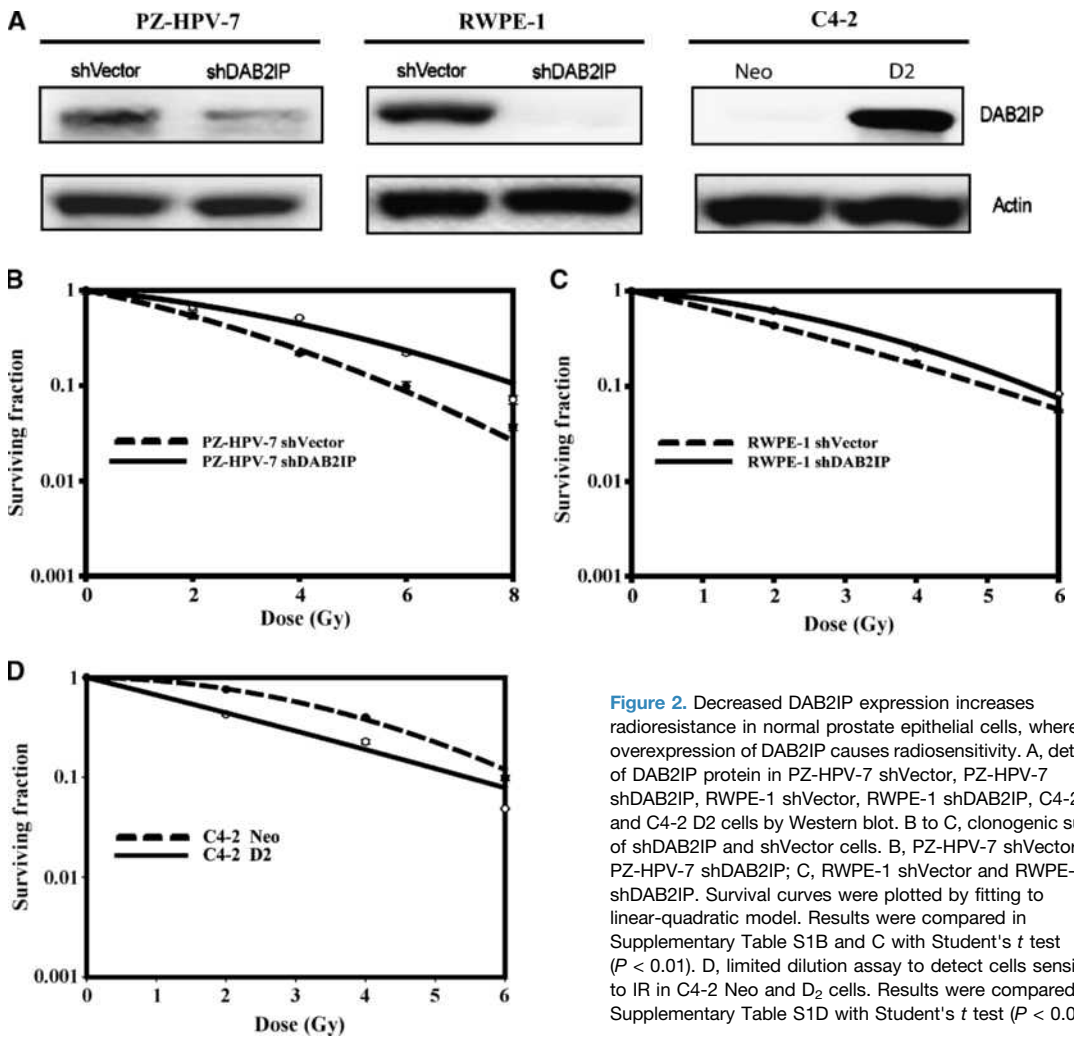

Figure 2. Decreased DAB2IP expression increases radioresistance in normal prostate epithelial cells, whereas overexpression of DAB2IP causes radiosensitivity. A, detection of DAB2IP protein in PZ-HPV-7 shVector, PZ-HPV-7 shDAB2IP, RWPE-1 shVector, RWPE-1 shDAB2IP, C4-2 Neo, and C4-2 D2 cells by Western blot. B to C, clonogenic survival of shDAB2IP and shVector cells. B, PZ-HPV-7 shVector and PZ-HPV-7 shDAB2IP; C, RWPE-1 shVector and RWPE-1 shDAB2IP. Survival curves were plotted by fitting to linear-quadratic model. Results were compared in Supplementary Table S1B and C with Student's *t* test ($P < 0.01$). D, limited dilution assay to detect cells sensitivity to IR in C4-2 Neo and D_2 cells. Results were compared in Supplementary Table S1D with Student's *t* test ($P < 0.01$).

Downloaded from http://aacrjournals.org/cancerres/article-pdf/70/7/2829/2645522/2829.pdf by guest on 16 January 2025

Discussion

DAB2IP, also known as ASK-interacting protein 1 (20) and a potential tumor suppressor gene, is a novel member of the Ras GTPase–activating protein family and plays an important role in balancing intracellular proliferation, survival, and apoptosis (5, 21). Loss of DAB2IP expression is often observed in prostate cancer cells (5) and is associated with

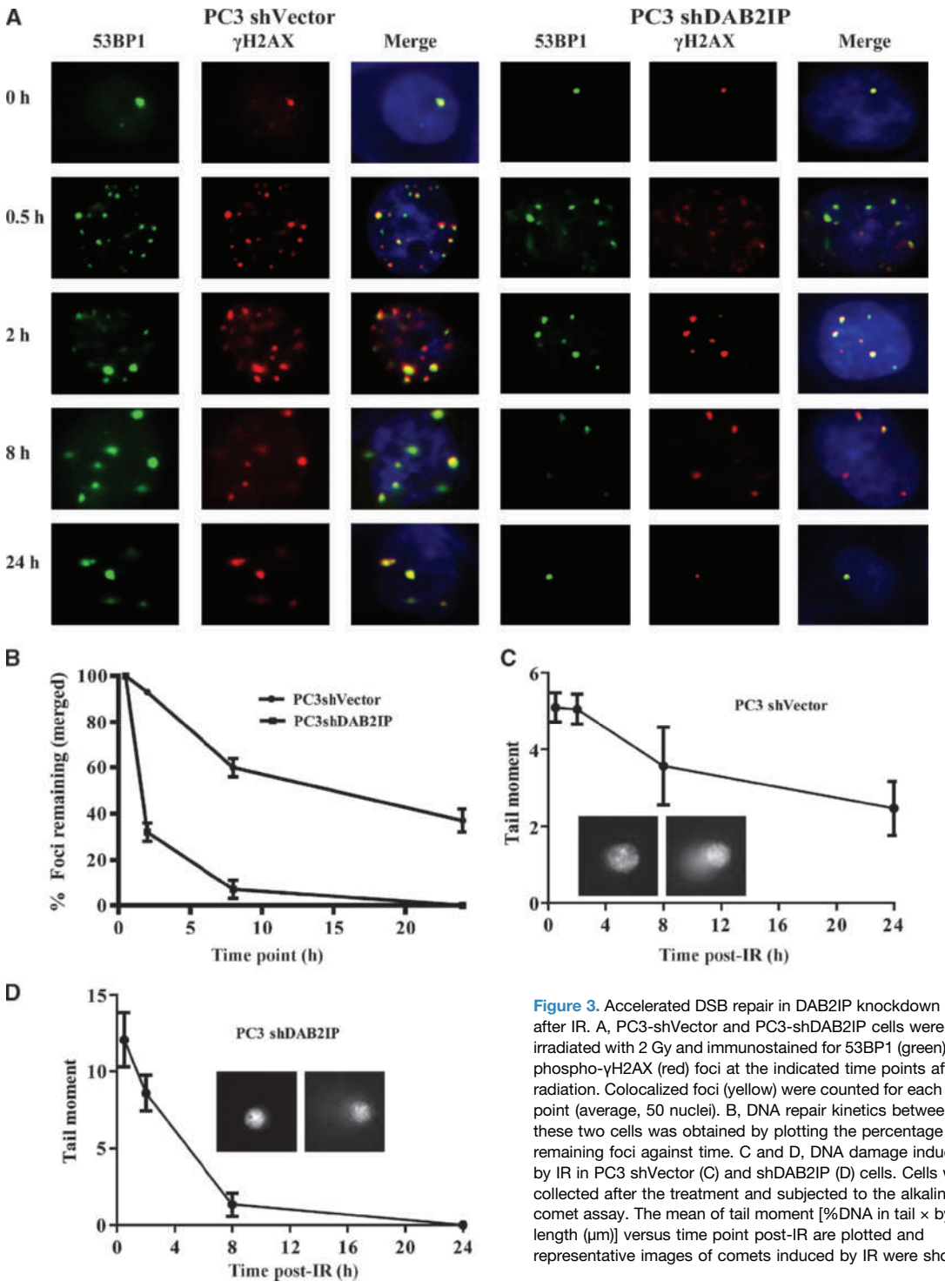

Figure 3. Accelerated DSB repair in DAB2IP knockdown cells after IR. A, PC3-shVector and PC3-shDAB2IP cells were irradiated with 2 Gy and immunostained for 53BP1 (green) and phospho-γH2AX (red) foci at the indicated time points after radiation. Colocalized foci (yellow) were counted for each time point (average, 50 nuclei). B, DNA repair kinetics between these two cells was obtained by plotting the percentage of remaining foci against time. C and D, DNA damage induced by IR in PC3 shVector (C) and shDAB2IP (D) cells. Cells were collected after the treatment and subjected to the alkaline comet assay. The mean of tail moment [%DNA in tail × by tail length (μm)] versus time point post-IR are plotted and representative images of comets induced by IR were shown.

Downloaded from http://aacrjournals.org/cancerres/article-pdf/70/7/2829/2645522/2829.pdf by guest on 16 January 2025

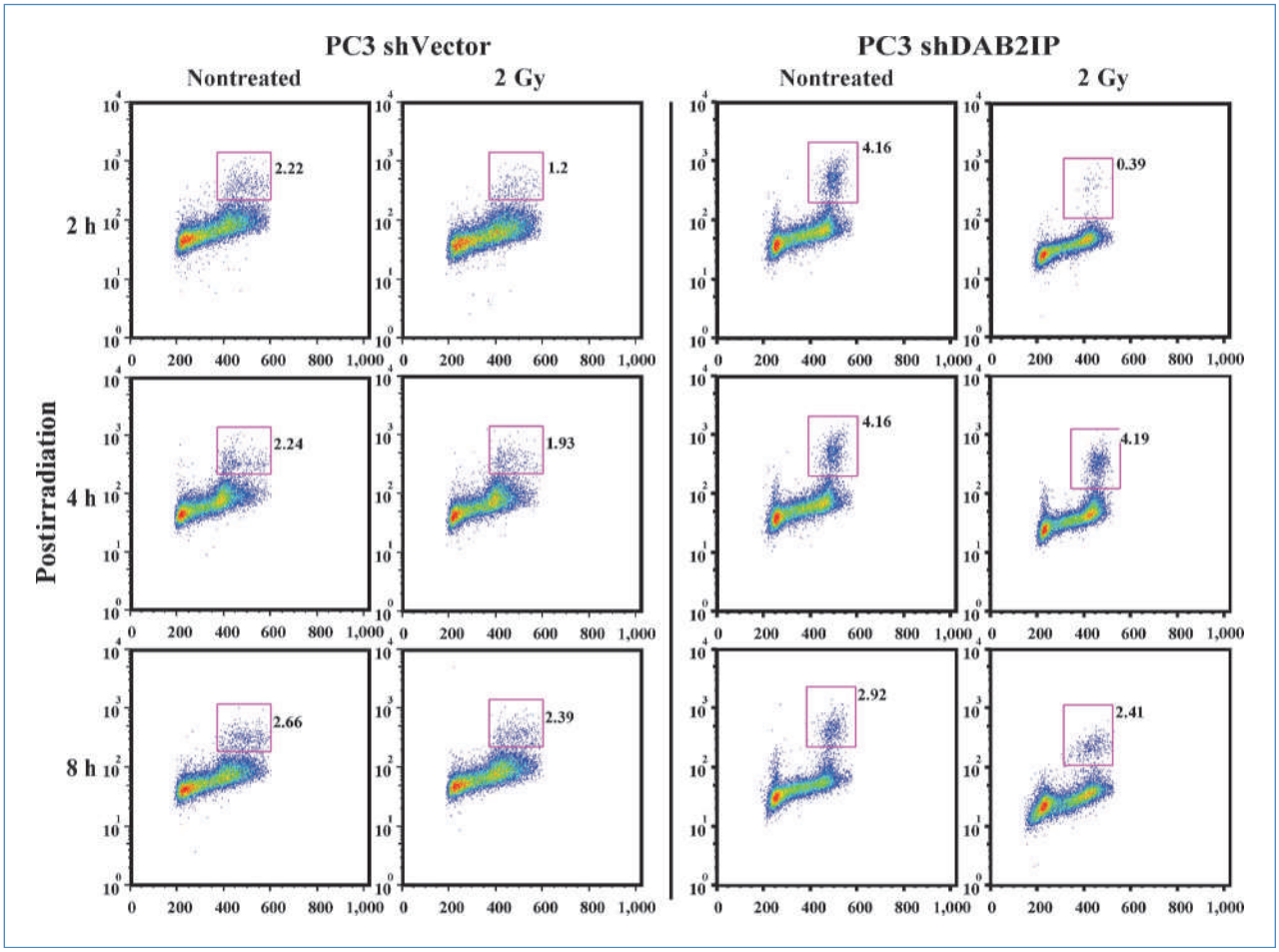

Figure 4. DAB2IP knockdown cells exhibit a robust early G_2-M checkpoint after IR. Early G_2-M checkpoint in PC3 shVector and PC3 shDAB2IP cells was assayed by flowcytometric analysis using PI staining for DNA content and anti–phospho-Histone H3 for detecting the % of mitosis cells. Cells were irradiated at 2 Gy and samples were collected 2, 4, and 8 h postradiation. Inset, the % of mitosis cells.

increased risk of tumor metastasis. A similar relationship between DAB2IP expression and aggressive tumor is also reported in breast cancer (22). Depletion of DAB2IP in prostate cancer cells as well as normal prostate epithelia leads to phosphoinositide 3-kinase-Akt, mitogen-activated protein kinase activation, and ASK1-c-Jun NH_2-kinase inactivation by which cells become resistant to stress-induced apoptosis (6). Nevertheless, this is the first study to report that the loss of DAB2IP expression in prostate cells contributes to the resistance to IR. We believe that an accelerated process of DNA DSB repair, a robust G_2-M checkpoint, and a functional system to escape from apoptosis are the underlying mechanisms. It is well known that the loss of certain genes such as PTEN and ATM markedly alters radiation responses. Mutational or epigenetic inactivation of PTEN results in constitutive activation of Akt and its downstream substrates, and as a result, cells are resistant to apoptosis and IR, whereas ectopic expression of PTEN causes radiosensitization (23–25). In prostate cancer, PTEN loss (~70%) has been associated with progression to androgen independence, chemoresistance, radioresistance, and bone metastasis (26–28). On the other hand, alteration in ATM expression is frequently reported in prostate tumorigenesis and the enhanced ATM levels could be correlated with the elevated level of prostate-specific antigen (29, 30). Further experiments are needed to elucidate whether DAB2IP may exert its effects by intersecting with pathways regulated by PTEN or ATM.

IR can cause a variety of DNA damage, including base lesions, DNA-protein cross-links, single-strand breaks, and DSBs, of which DSBs are the most potent, resulting in cell death or genomic instability that could lead to carcinogenesis (31). The kinetics of residual phospho-γH2AX and 53BP1-colocalized foci in shDAB2IP and shVector cells represent a significant difference in the kinetics of DSB repair. H2AX phosphorylation has also been reported to occur under conditions of cell stress such as hyperthermia (23). In addition to H2AX phosphorylation, accumulation of 53BP1 also occurs at the sites of DSBs and 53BP1 foci colocalized with IR-induced Mre11/NBS and H2AX foci; thus in addition to γH2AX foci, 53BP1 foci are also frequently used as a measure of DNA DSB repair kinetics (9, 10, 32). In these assays, the initial number of foci counted 30 minutes post-IR was similar for the both

Downloaded from http://aacrjournals.org/cancerres/article-pdf/70/7/2829/2645522/2829.pdf by guest on 16 January 2025

cell lines. Hence, the differences in repair kinetics are not caused by any difference in the initial damage. For the sake of quantitative accuracy, we have used both γH2AX and 53BP1 foci as surrogate markers for DSBS, and based on this and results from a Comet assay, we show the faster repair kinetics of shDAB2IP cells is a major contributing factor toward radioresistance. Similar to our results, previous reports by Mukherjee and colleagues (33) and Golding and colleagues (34) showed the increased glioblastoma multiforme radioresistance is due to augmented DSB repair kinetics. At this point, the mechanism of accelerated DSB repair in DAB2IP-deficient cells is under investigation.

Cell cycle checkpoint is another defense mechanism to protect cells from DNA damage allowing them to repair

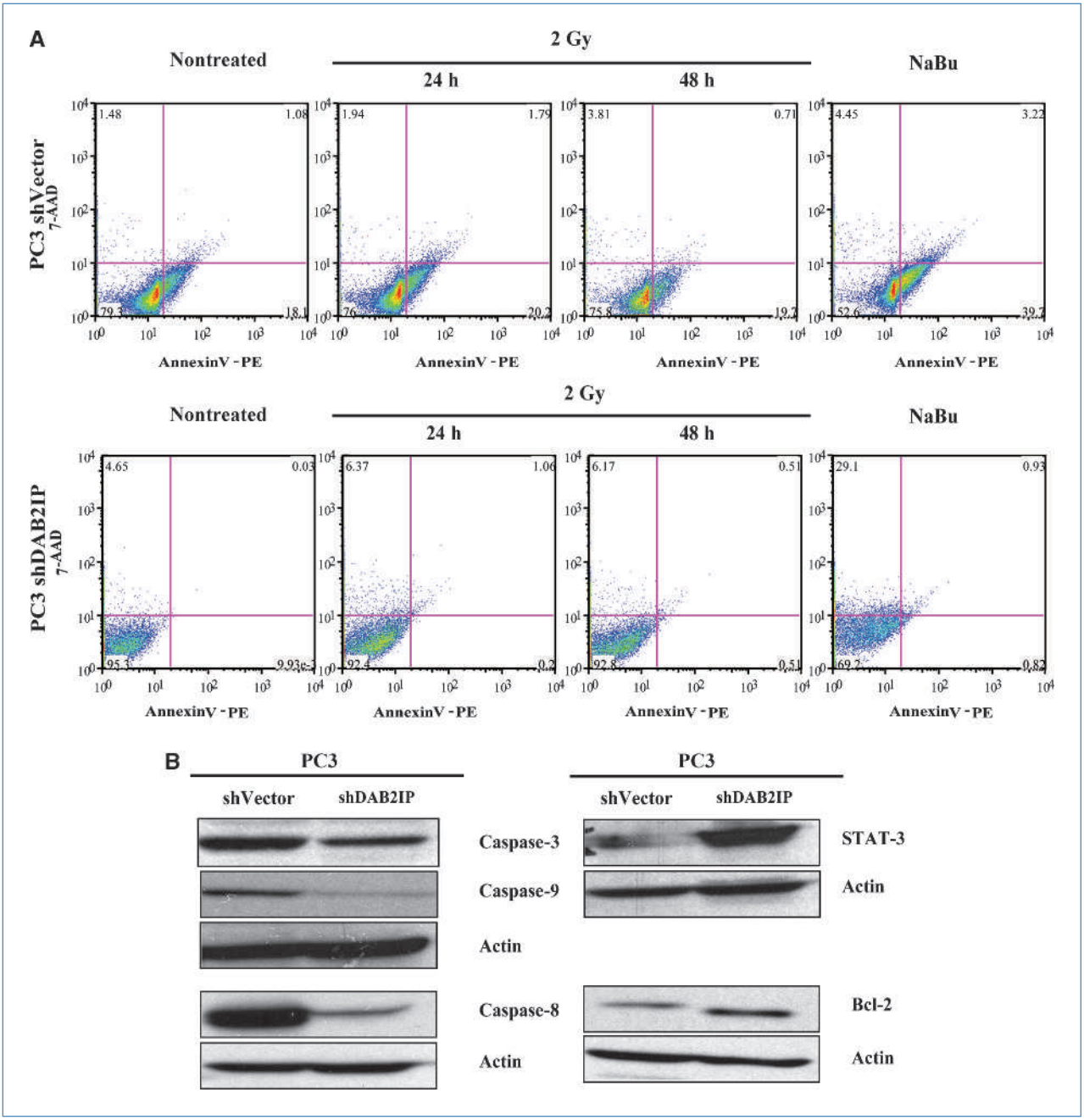

Figure 5. DAB2IP knockdown cells exhibit resistance to radiation-induced apoptosis. A, radiation-induced apoptotic responses in these two cells were determined by flow cytometry using Annexin V/7-AAD staining kit. These cells were treated with 2 Gy IR and the samples were collected 24 and 48 h post-IR; the proportion of apoptosis cells were detected by Flowjo 8.7.1. NaBu was used as positive control for cell death. B, Western blot analysis of proapoptotic and antiapoptotic proteins in PC3 shVector and PC3 shDAB2IP cells. Unirradiated cells were lysed and subjected to Western blot analysis for caspase-3, caspase-8, caspase-9, Bcl-2, and STAT3.

Downloaded from http://aacrjournals.org/cancerres/article-pdf/70/7/2829/2645522/2829.pdf by guest on 16 January 2025

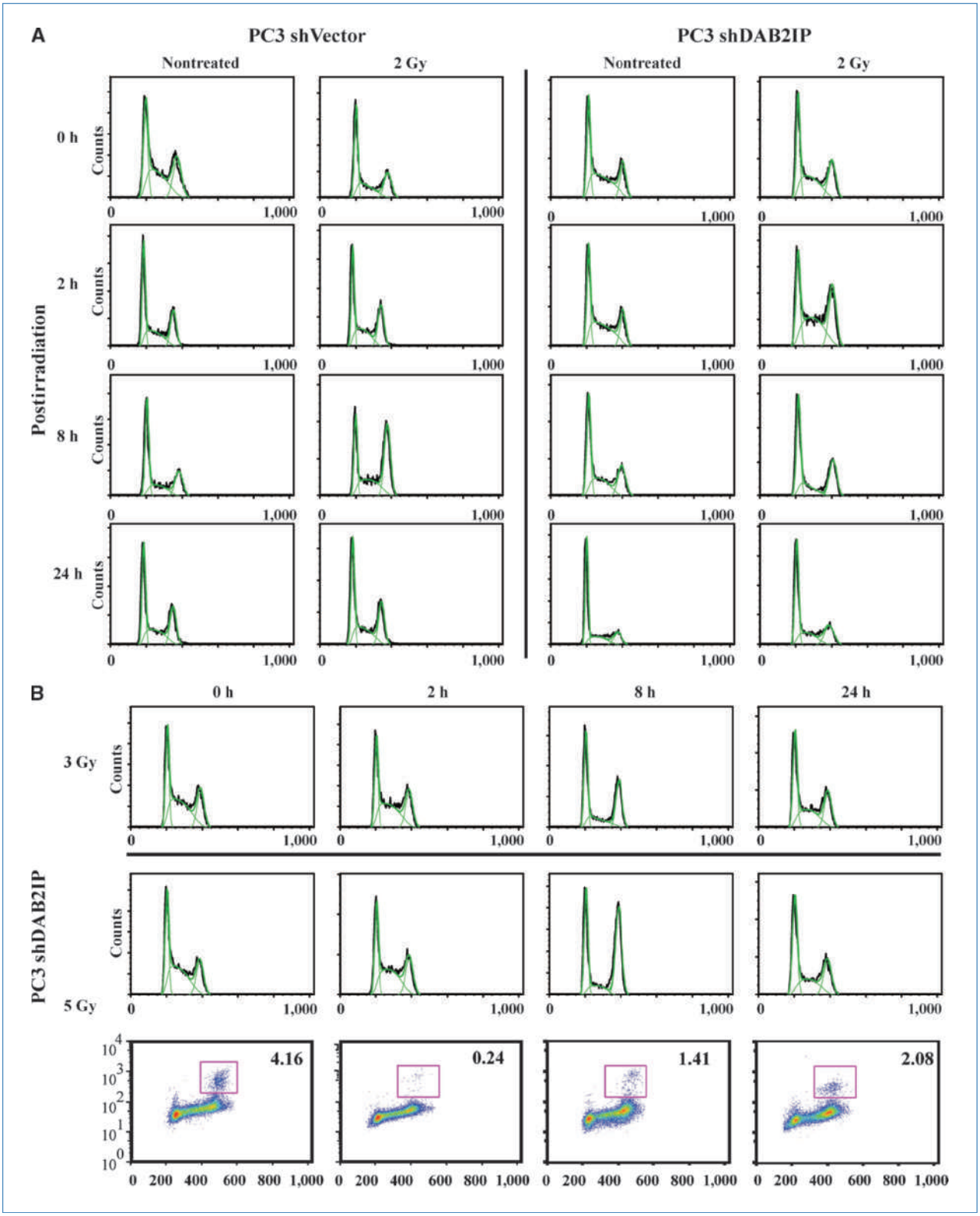

Figure 6. A dosage-dependent G_2-M arrest in DAB2IP knockdown cells after IR. A, PC3 shVector and PC3 shDAB2IP were treated with 2 Gy and collected 0, 2, 8, and 24 h postradiation. PI staining was applied to detect the distribution of cell cycle response to ionizing irradiation by flow cytometry. B, PC3 shDAB2IP cells were exposed to 3 Gy (top) and 5 Gy (middle, PI staining only; bottom, phospho-histone-H3 and PI dual-staining for mitosis cells), respectively. The DNA profiles were obtained 0, 2, 8, and 24 h after irradiation.

Downloaded from http://aacrjournals.org/cancerres/article-pdf/70/7/2829/2645522/2829.pdf by guest on 16 January 2025

genetic lesions (35, 36). Radiation-induced G_2 arrest is critical in preventing cells from death (37). In this study, two distinct G_2 arrests were noticed in shDAB2IP and shVector cells in response to IR. shDAB2IP deficient cells showed early G_2 checkpoint within 2 hours (Fig. 4), whereas control shVector cells exhibit late G_2 arrest 8 hours after radiation (Fig. 6A). shDAB2IP cells did not exhibit late G_2 arrest until a higher radiation dose (5 Gy) was used (Fig. 6B).

In an additional experiment, we monitored S-phase population using bromodeoxyuridine (BdrUrd) in shDAB2IP cells following IR (Supplementary Fig. S2). S-phase cells were labeled with BrdUrd for 30 minutes before 2 Gy radiation. After 8 hours, >90% BrdUrd-positive cells (both treated and nontreated) entered either G1 or S phase of the following cell cycle (Supplementary Fig. S2A and B). In contrast, at 5 Gy, a large proportion (>50%) of BrdUrd-positive shDAB2IP cells were blocked at G_2 at the same time point (Supplementary Fig. S2C), indicating that these cells are still undergoing DSB repair. Therefore, at 5 Gy, the late G_2 arrest in shDA2IP cells resulted from the unrepaired S population that is blocked at G_2.

Apoptosis is an important mechanism by which IR exerts its therapeutic response (38, 39) and faulty apoptosis is a known mechanism leading to resistance to radiation therapy. Preclinical studies showed that wild-type p53 was required for apoptosis induced by IR; however, many clinical outcomes clearly indicated that p53 status was not a useful prognostic marker for successful radiation therapy (40, 41). Both shDAB2IP deficient and vector shVector controlled cells were derived from the parental PC3 cells bearing p53 mutation and PTEN deletion (42–44). It is known that caspase family and Bcl-2 family are the major families involved in apoptosis. Caspase-8 and caspase-9 are associated with activating "extrinsic" and "intrinsic" apoptosis pathway (45), respectively, and caspase-3 is the critical executioner to participating in both apoptosis process (46). On the other hand, Bcl-2 is the key antiapoptotic protein and is induced by STAT3 (47, 48). In this study, we compared the expression of caspase-3, caspase-8, caspase-9, Bcl-2, and STAT3 in shDAB2IP and shVector cells. The results support the observation that shDABIP cells are resistant to apoptosis as the levels of proapoptotic proteins caspase-3, caspase-8, and caspase-9 are significantly lower than shVector cells. In contrast, antiapoptotic proteins such as Bcl-2 and STAT3 levels are higher in shDAB2IP cells; overexpression of both Bcl-2 and STAT3 has been reported to be associated with radioresistance (49–51). Although the mechanism(s) leading to increased expression of antiapoptotic protein levels or decreased expression of proapoptotic proteins in shDAB2IP cells is largely unknown, we hypothesize that DAB2IP could modulate the half-life of these proteins through proteasomal degradation as previously found (6). However, we cannot rule out that DAB2IP may function through transcriptional regulation. Nevertheless, these data strongly support that the loss of DAB2IP in prostate cell confers a survival advantage to IR due to enhanced DSB repair, strong G_2-M checkpoint control, and evasion of apoptosis. Therefore, identifying individual patients with dysregulated DAB2IP gene is of significant clinical importance.

Disclosure of Potential Conflicts of Interest

No potential conflicts of interest were disclosed.

Grant Support

Flight Attendant Medical Research Institute (D. Saha and J.T. Hsieh), NASA Grants NNA05CS97G and NNX10AE08G (S. Burma), CA 050519 to (D.J. Chen), and the Cancer Prevention and Research Institute of Texas (RP100644 to S. Burma).

The costs of publication of this article were defrayed in part by the payment of page charges. This article must therefore be hereby marked *advertisement* in accordance with 18 U.S.C. Section 1734 solely to indicate this fact.

Received 08/07/2009; revised 12/31/2009; accepted 01/13/2010; published OnlineFirst 03/23/2010.

References

1. Jemal A, Siegel R, Ward E, et al. Cancer statistics, 2008. CA Cancer J Clin 2008;58:71–96.
2. Hanks GE, Pajak TF, Porter A, et al. Phase III trial of long-term adjuvant androgen deprivation after neoadjuvant hormonal cytoreduction and radiotherapy in locally advanced carcinoma of the prostate: the Radiation Therapy Oncology Group Protocol 92-02. J Clin Oncol 2003;21:3972–8.
3. Thompson IM, Tangen CM, Paradelo J, et al. Adjuvant radiotherapy for pathological T3N0M0 prostate cancer significantly reduces risk of metastases and improves survival: long-term followup of a randomized clinical trial. J Urol 2009;181:956–62.
4. Duggan D, Zheng SL, Knowlton M, et al. Two genome-wide association studies of aggressive prostate cancer implicate putative prostate tumor suppressor gene DAB2IP. J Natl Cancer Inst 2007;99:1836–44.
5. Chen H, Pong RC, Wang Z, Hsieh JT. Differential regulation of the human gene DAB2IP in normal and malignant prostatic epithelia: cloning and characterization. Genomics 2002;79:573–81.
6. Xie D, Gore C, Zhou J, et al. DAB2IP coordinates both PI3K-Akt and ASK1 pathways for cell survival and apoptosis. Proc Natl Acad Sci U S A 2009;106:19878–83.
7. Xie D, Gore C, Liu J, et al. Role of DAB2IP in modulating epithelial-to-mesenchymal transition and prostate cancer metastasis. Proc Natl Acad Sci U S A 2010;107:2485–90.
8. Green MH, Arlett CF, Cole J, et al. Comparative human cellular radiosensitivity: III. γ-radiation survival of cultured skin fibroblasts and resting T-lymphocytes from the peripheral blood of the same individual. Int J Radiat Biol 1991;59:749–65.
9. Rappold I, Iwabuchi K, Date T, Chen J, et al. Tumor suppressor p53 binding protein 1 (53BP1) is involved in DNA damage-signaling pathways. J Cell Biol 2001;153:613–20.
10. Schultz LB, Chehab NH, Malikzay A, Halazonetis TD. p53 binding protein 1 (53BP1) is an early participant in the cellular response to DNA double-strand breaks. J Cell Biol 2000;151:1381–90.
11. Huang H, Reed CP, Zhang JS, Shridhar V, Wang L, Smith DI. Carboxypeptidase A3 (CPA3): a novel gene highly induced by histone deacetylase inhibitors during differentiation of prostate epithelial cancer cells. Cancer Res 1999;59:2981–8.
12. Saha D, Datta PK, Sheng H, et al. Synergistic induction of cyclooxygenase-2 by transforming growth factor-β1 and epidermal growth factor inhibits apoptosis in epithelial cells. Neoplasia 1999;1:508–17.

Downloaded from http://aacrjournals.org/cancerres/article-pdf/70/7/2829/2645522/2829.pdf by guest on 16 January 2025

13. Foray N, Arlett CF, Malaise EP. Radiation-induced DNA double-strand breaks and the radiosensitivity of human cells: a closer look. Biochimie 1997;79:567–75.
14. Nunez MI, McMillan TJ, Valenzuela MT, Ruiz de Almodovar JM, Pedraza V. Relationship between DNA damage, rejoining and cell killing by radiation in mammalian cells. Radiother Oncol 1996;39: 155–65.
15. Asaithamby A, Chen DJ. Cellular responses to DNA double-strand breaks after low-dose γ-irradiation. Nucleic Acids Res 2009;37:3912–23.
16. Burma S, Chen BP, Murphy M, Kurimasa A, Chen DJ. ATM phosphorylates histone H2AX in response to DNA double-strand breaks. J Biol Chem 2001;276:42462–7.
17. Kobayashi J, Tauchi H, Chen B, et al. Histone H2AX participates the DNA damage-induced ATM activation through interaction with NBS1. Biochem Biophys Res Commun 2009;380:752–7.
18. Olive PL, Banath JP. The comet assay: a method to measure DNA damage in individual cells. Nat Protoc 2006;1:23–9.
19. Tomimatsu N, Mukherjee B, Burma S. Distinct roles of ATR and DNA-PKcs in triggering DNA damage responses in ATM-deficient cells. EMBO Rep 2009;10:629–35.
20. Zhang H, Zhang R, Luo Y, D'Alessio A, Pober JS, Min W. AIP1/DAB2IP, a novel member of the Ras-GAP family, transduces TRAF2-induced ASK1-JNK activation. J Biol Chem 2004;279:44955–65.
21. Chen H, Karam JA, Schultz R, Zhang Z, Duncan C, Hsieh JT. Cloning of mouse Dab2ip gene, a novel member of the RasGTPase-activating protein family and characterization of its regulatory region in prostate. DNA Cell Biol 2006;25:232–45.
22. Dote H, Toyooka S, Tsukuda K, et al. Aberrant promoter methylation in human DAB2 interactive protein (hDAB2IP) gene in breast cancer. Clin Cancer Res 2004;10:2082–9.
23. Gupta A, Yang Q, Pandita RK, et al. Cell cycle checkpoint defects contribute to genomic instability in PTEN deficient cells independent of DNA DSB repair. Cell Cycle 2009;8:2198–210.
24. Kao GD, Jiang Z, Fernandes AM, Gupta AK, Maity A. Inhibition of phosphatidylinositol-3-OH kinase/Akt signaling impairs DNA repair in glioblastoma cells following ionizing radiation. J Biol Chem 2007;282:21206–12.
25. Pappas G, Zumstein LA, Munshi A, Hobbs M, Meyn RE. Adenoviral-mediated PTEN expression radiosensitizes non-small cell lung cancer cells by suppressing DNA repair capacity. Cancer Gene Ther 2007;14:543–9.
26. Anai S, Goodison S, Shiverick K, Iczkowski K, Tanaka M, Rosser CJ. Combination of PTEN gene therapy and radiation inhibits the growth of human prostate cancer xenografts. Hum Gene Ther 2006;17: 975–84.
27. Shen MM, Abate-Shen C. Pten inactivation and the emergence of androgen-independent prostate cancer. Cancer Res 2007;67: 6535–8.
28. Wu Z, McRoberts KS, Theodorescu D. The role of PTEN in prostate cancer cell tropism to the bone micro-environment. Carcinogenesis 2007;28:1393–400.
29. Angele S, Falconer A, Foster CS, Taniere P, Eeles RA, Hall J. ATM protein overexpression in prostate tumors: possible role in telomere maintenance. Am J Clin Pathol 2004;121:231–6.
30. Truman JP, Gueven N, Lavin M, et al. Down-regulation of ATM protein sensitizes human prostate cancer cells to radiation-induced apoptosis. J Biol Chem 2005;280:23262–72.
31. Kobayashi J, Iwabuchi K, Miyagawa K, et al. Current topics in DNA double-strand break repair. J Radiat Res (Tokyo) 2008;49:93–103.
32. Fernandez-Capetillo O, Chen HT, Celeste A, et al. DNA damage-induced G_2-M checkpoint activation by histone H2AX and 53BP1. Nat Cell Biol 2002;4:993–7.
33. Mukherjee B, McEllin B, Camacho CV, et al. EGFRvIII and DNA double-strand break repair: a molecular mechanism for radioresistance in glioblastoma. Cancer Res 2009;69:4252–9.
34. Golding SE, Morgan RN, Adams BR, Hawkins AJ, Povirk LF, Valerie K. Pro-survival AKT and ERK signaling from EGFR and mutant EGFRvIII enhances DNA double-strand break repair in human glioma cells. Cancer Biol Ther 2009;8:730–8.
35. Bernhard EJ, Maity A, Muschel RJ, McKenna WG. Effects of ionizing radiation on cell cycle progression. A review. Radiat Environ Biophys 1995;34:79–83.
36. Xu B, Kim ST, Lim DS, Kastan MB. Two molecularly distinct G(2)/M checkpoints are induced by ionizing irradiation. Mol Cell Biol 2002; 22:1049–59.
37. Teyssier F, Bay JO, Dionet C, Verrelle P. [Cell cycle regulation after exposure to ionizing radiation]. Bull Cancer 1999;86:345–57.
38. An J, Chervin AS, Nie A, Ducoff HS, Huang Z. Overcoming the radioresistance of prostate cancer cells with a novel Bcl-2 inhibitor. Oncogene 2007;26:652–61.
39. Denmeade SR, Lin XS, Isaacs JT. Role of programmed (apoptotic) cell death during the progression and therapy for prostate cancer. Prostate 1996;28:251–65.
40. Langendijk JA, Thunnissen FB, Lamers RJ, de Jong JM, ten Velde GP, Wouters EF. The prognostic significance of accumulation of p53 protein in stage III non-small cell lung cancer treated by radiotherapy. Radiother Oncol 1995;36:218–24.
41. Prendergast NJ, Atkins MR, Schatte EC, Paulson DF, Walther PJ. p53 immunohistochemical and genetic alterations are associated at high incidence with post-irradiated locally persistent prostate carcinoma. J Urol 1996;155:1685–92.
42. Bouali S, Chretien AS, Ramacci C, et al. P53 and PTEN expression contribute to the inhibition of EGFR downstream signaling pathway by cetuximab. Cancer Gene Ther 2009;16:498–507.
43. Carroll AG, Voeller HJ, Sugars L, Gelmann EP. p53 oncogene mutations in three human prostate cancer cell lines. Prostate 1993;23: 123–34.
44. Isaacs WB, Carter BS, Ewing CM. Wild-type p53 suppresses growth of human prostate cancer cells containing mutant p53 alleles. Cancer Res 1991;51:4716–20.
45. Papandile A, Tyas D, O'Malley DM, Warner CM. Analysis of caspase-3, caspase-8 and caspase-9 enzymatic activities in mouse oocytes and zygotes. Zygote 2004;12:57–64.
46. Mazumder S, Plesca D, Almasan A. Caspase-3 activation is a critical determinant of genotoxic stress-induced apoptosis. Methods Mol Biol 2008;414:13–21.
47. Choi HJ, Lee JH, Park SY, Cho JH, Han JS. STAT3 is involved in phosphatidic acid-induced Bcl-2 expression in HeLa cells. Exp Mol Med 2009;41:94–101.
48. Kim SR, Bae MK, Kim JY, Wee HJ, Yoo MA, Bae SK. Aspirin induces apoptosis through the blockade of IL-6-STAT3 signaling pathway in human glioblastoma A172 cells. Biochem Biophys Res Commun 2009;387:342–7.
49. Aggarwal BB, Sethi G, Ahn KS, et al. Targeting signal-transducer-and-activator-of-transcription-3 for prevention and therapy of cancer: modern target but ancient solution. Ann N Y Acad Sci 2006;1091:151–69.
50. Krajewska M, Krajewski S, Epstein JI, et al. Immunohistochemical analysis of bcl-2, bax, bcl-X, mcl-1 expression in prostate cancers. Am J Pathol 1996;148:1567–76.
51. Rosser CJ, Reyes AO, Vakar-Lopez F, et al. Bcl-2 is significantly overexpressed in localized radio-recurrent prostate carcinoma, compared with localized radio-naive prostate carcinoma. Int J Radiat Oncol Biol Phys 2003;56:1–6.

Downloaded from http://aacrjournals.org/cancerres/article-pdf/70/7/2829/2645522/2829.pdf by guest on 16 January 2025